

Measurement of atomic-hydrogen diffusion in helium

S. G. Redsun and R. J. Knize

Department of Physics and Plasma Physics Laboratory, Princeton University, Princeton, New Jersey 08544

(Received 24 June 1987)

The diffusion constant of atomic hydrogen in helium gas, $D_0(\text{H-He})$, was measured with use of an optical-pumping–spin-exchange technique. Atomic hydrogen was produced by an inductive discharge in spherical Pyrex cells containing helium and small amounts of molecular hydrogen (<2%) and rubidium. The rubidium was optically pumped by a vapor lamp and the hydrogen was polarized by subsequent spin-exchange collisions. The decay rate of the hydrogen concentration was obtained from the observed time dependence of the hydrogen Zeeman signal and the diffusion constant was determined by measuring the decay rate in cells of different radius and helium pressure. $D_0(\text{H-He})$ was found to be $2.42(7) \text{ cm}^2 \text{ sec}^{-1}$ at 60°C , which may be extrapolated to $1.70(5) \text{ cm}^2 \text{ sec}^{-1}$ at 0°C . This result is significantly more accurate and more consistent with theoretical calculations than the results of previous experiments.

I. INTRODUCTION

Accurate experimental measurements of atomic-hydrogen diffusion in helium allow improvement of current physical models of such systems as the upper atmosphere, electric discharge plasmas, molecular transport in fusion reactors,¹ and cryogenic hydrogen masers with liquid-helium-coated walls.² The H-He system is of considerable interest because its interaction potential is among the simplest interatomic potentials and has one of the smallest well depths of all neutral diatoms, comparable to that of two spin-polarized hydrogen atoms ($\sim 0.5 \text{ meV}$).³ Of secondary interest is the fact that these atoms are so small that quantum effects (e.g., diffraction of the wave functions) which modify their diffusion are not negligible even at room temperature.⁴

Most techniques for measuring room-temperature hydrogen diffusion make use of the fact that the wall recombination rate of free hydrogen atoms is modified by their diffusion in the surrounding gas. By measuring quantities dependent on the time-varying atomic hydrogen concentration $[\text{H}]$, such as magnetic resonance linewidths⁵ or the intensity of plasma-induced electronic transitions,⁶ the diffusion constant may be determined indirectly. It is difficult to measure the hydrogen concentration by direct spectroscopic methods because electronic transitions between the ground state and excited states of the hydrogen atom lie in the vacuum-ultraviolet spectrum, where efficient light sources, lenses, windows, polarizers, and other optical components are difficult to obtain.⁷

In this paper the diffusion constant of atomic hydrogen in helium was determined using optical pumping of rubidium, subsequent spin exchange with hydrogen atoms, and measurement of the decay rate of the atomic-hydrogen concentration. Although Rb-H spin exchange in the presence of a buffer gas has previously been investigated,⁸ this technique has only recently been employed to measure diffusion.⁹ This method is relatively free of systematic errors and allows determination of

the diffusion constant at room temperature to within a few percent accuracy (which is comparable to the accuracy obtained by spin-echo techniques at liquid-helium temperatures¹⁰). This technique may be used to measure diffusion of other difficult atomic species such as nitrogen, and also to differentiate between isotopes with different nuclear spin, such as hydrogen and deuterium.

In subsequent sections of this paper we will discuss the experimental apparatus and technique, the theory of diffusion and how the diffusion rate is related to the observed signal, the treatment of experimental uncertainties, the experimental results and their comparison to previous experiments and theoretical calculations, and our conclusions.

II. EXPERIMENTAL APPARATUS

Spherical Pyrex cells with diameters of 2–5 cm were cleansed thoroughly in an inductive discharge (using a ~ 1 -torr H_2 -He mixture) and heated with a natural-gas flame to drive off absorbed water vapor and other impurities while they were evacuated below 10^{-6} torr. The cells were subsequently filled with molecular hydrogen, helium, and several small droplets of natural rubidium.

The alkali-metal and hydrogen polarizations are not significantly affected by the presence of helium and hydrogen buffer gases at the presence used in this experiment.⁷ However, the buffer gas will retard the rate at which hydrogen atoms diffuse to the cell walls, where they depolarize and recombine. At low helium pressures, the rubidium and hydrogen atoms diffuse quickly to the walls and relax so rapidly that their polarizations are small. If the helium pressure is too high, the discharge is unable to break down the gas and create hydrogen atoms. Hence the cells were filled at room temperature to a helium partial pressure between 21 and 51 torr and a hydrogen partial pressure between 0.41 and 0.55 torr. The pressure was measured with a capacitance manometer with an accuracy of about 0.02 torr. The manufacturer's stated purity was greater than

99.9995% for both gases.¹¹

The experimental apparatus is shown schematically in Fig. 1. A rubidium vapor lamp¹² is used to illuminate the cell. The light is first passed through an interference filter to select the rubidium D_1 resonance line ($\lambda=794.8$ nm) and is then circularly polarized by a linear polarizer and a quarter-wave plate. A spherical lens focuses the light into the cell, polarizing the rubidium atoms by optical pumping.⁷

The cell itself is situated in a thermally insulated oven with glass windows. Hot air piped into the oven heats the cell to a temperature of about 60°C, and the rubidium number density may be determined from published vapor-pressure curves.¹³ Because the rubidium vapor pressure is less than 10^{-2} torr at the temperatures used in this experiment, the presence of rubidium has a negligible effect on hydrogen diffusion. The oven temperature was measured by a copper-Constantan thermocouple mounted near the cell and was found to remain constant to within a few degrees for all measurements.

Atomic hydrogen is produced by a pulsed radio-frequency (rf) inductive discharge (~ 21 MHz, ~ 50 W) applied to the cell and becomes polarized by spin-exchange collisions with the optically pumped rubidium atoms. External Helmholtz coils (not shown in Fig. 1) maintain a uniform magnetic field ($B \sim 1$ G) in the direction of the light, which also defines the spin-polarization axis. Auxiliary coils are operated at the frequency

$$f \approx \frac{g\mu_B B}{h(2I+1)}, \quad (1)$$

where $g \approx 2$ is the electron g factor, h is Planck's constant, and μ_B is the Bohr magneton, to depolarize atoms of nuclear spin I by inducing Zeeman transitions ($\Delta F=0$, $\Delta m_F = \pm 1$) between adjacent hyperfine sublevels. The energy difference between adjacent sublevels is nearly linear in B at such low magnetic fields, so Eq. (1) is an excellent approximation. The oven is electrically shielded in order to avoid pickup of the discharge rf by the detection electronics, and the apparatus contains no magnetic materials which could cause depolarization.

The transmitted light is collimated by a second spherical lens and detected by a silicon photodetector. If the rubidium is unpolarized at a given time, some of the photons will be absorbed and the cell will be partially

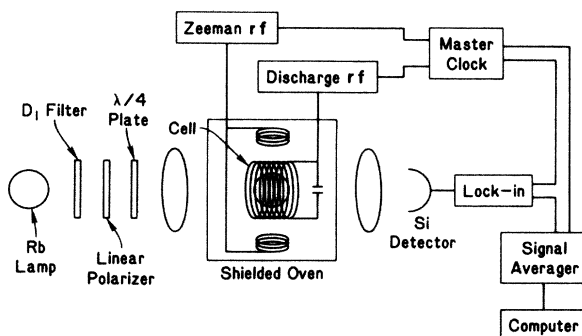


FIG. 1. Schematic diagram of the experimental apparatus.

opaque to the light. As the rubidium polarization increases, the cell becomes more transparent to the light. Hence the light transmission is related to the degree of polarization of the rubidium. The detector output is sent to a lock-in amplifier.

Figure 2 shows the unique timing sequence used in this experiment. The master clock defines two equal half-cycles of duration $\tau_c/2$ (~ 40 – 130 msec), each of which begins with a discharge pulse ($\tau_d \sim 100$ μ sec). During one half-cycle the rubidium and hydrogen polarizations are allowed to evolve normally following the discharge pulse. During the next half-cycle, the hydrogen atoms are completely depolarized by application of a short rf pulse ($\tau_z = 2$ msec) at the hydrogen ($I = \frac{1}{2}$) Zeeman frequency. This Zeeman pulse is delayed by a variable time t_0 from the end of the discharge pulse. The lock-in amplifier integrates the difference in the light transmission between these two half-cycles. The output of the lock-in amplifier is recorded with a signal averager while the delay time t_0 is increased from zero to $\tau_c/2$.

A plot of this signal as a function of the delay time t_0 is obtained by repeating this process several times, as shown in Fig. 3. After the initial signal buildup, the hydrogen atoms become polarized, and the signal decays exponentially due to the hydrogen atoms being lost to recombination at the cell wall (as will be shown in Sec. III). The exponential-decay part of this curve is analyzed to determine the decay constant τ^{-1} of the atomic-hydrogen concentration, from which the diffusion constant may be calculated.

III. THEORY

A. Diffusion

Classical diffusion theory predicts that under isothermal conditions the spatial and temporal evolution of the particle concentration $n(r, t)$ is governed by the familiar diffusion equation

$$D \nabla^2 n = \partial n / \partial t, \quad (2)$$

where D is the diffusion constant. If the particles are enclosed in a spherical cell (radius R) whose wall is a parti-

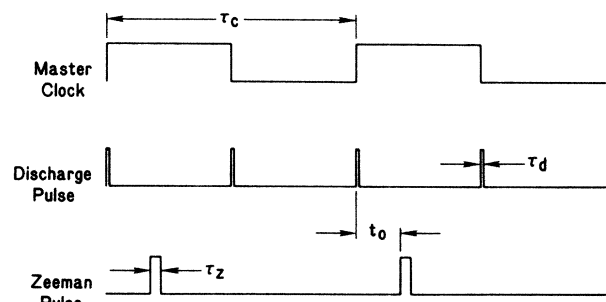


FIG. 2. Timing sequence showing the discharge (τ_d) and Zeeman (τ_z) pulse widths. The depolarizing Zeeman pulse can be delayed relative to the end of the discharge pulse by a variable time t_0 .

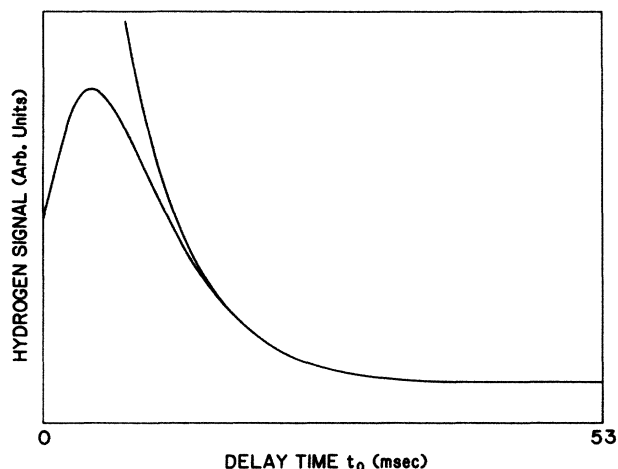


FIG. 3. Time evolution of an observed hydrogen signal. Once the atomic polarizations have had sufficient time to build up, the signal decays as $\exp[-(t_0/\tau)]$ due to recombination of hydrogen atoms at the cell wall.

cle sink [$n(R)=0$] due to wall recombination, the concentration may be expressed as a sum of exponentials which decay in time,

$$n(r,t) = \sum n_m(r) \exp(-t/\tau_m), \quad (3)$$

where τ_m is the recombination time constant and the subscript m refers to the order of the diffusion mode ($m=1,2,3,\dots$). The diffusion equation (2) for each mode reduces to

$$\frac{\partial^2 n_m}{\partial r^2} + \frac{2}{r} \frac{\partial n_m}{\partial r} + \frac{1}{D\tau_m} n_m = 0, \quad (4)$$

for which the solution is the spherical Bessel function of order zero:

$$n_m(r) = n_m(0) j_0(k_m r) = n_m(0) \frac{\sin(k_m r)}{k_m r}, \quad (5)$$

where $k_m \equiv (D\tau_m)^{-1/2}$. At the cell wall $n_m(R)=0$, which implies $k_m R = m\pi$,

$$\tau_m^{-1} = D_0 \frac{(m\pi)^2}{R^2} \frac{760 \text{ torr}}{P}, \quad (6)$$

where D_0 refers to the diffusion constant at 760 torr. Hence the particle recombination rate τ^{-1} in this experiment is directly related to the diffusion constant. It will be shown later that all except the slowest diffusion mode ($m=1$) may be neglected in this experiment, so we will adopt the convention $\tau \equiv \tau_1$ for the remainder of this report.

In this experiment there is multicomponent diffusion due to the presence of a small amount of molecular hydrogen in the helium buffer gas. The overall time constant τ is given by

$$\tau = \tau_{\text{H-He}} + \tau_{\text{H-H}_2} = \frac{R^2}{760\pi^2} \left[\frac{P_{\text{He}}}{D_0(\text{H-He})} + \frac{P_{\text{H}_2}}{D_0(\text{H-H}_2)} \right]. \quad (7)$$

$D_0(\text{H-H}_2)$ has been measured to be about $2.56 \text{ cm}^2 \text{ sec}^{-1}$ at 60°C ,^{9,14-16} so $D_0(\text{H-He})$ may be determined by measuring the recombination rate τ^{-1} and correcting for the small second term ($<3\%$) in Eq. (7).

Two other transport processes, viscous and free molecular flow,¹⁷ could also add to the diffusive flux $J_D = D\nabla n$ and modify the observed recombination rate. The viscous flow J_V due to pressure gradients in the cell of radius R is on the order of $nR^2\nabla p/\eta$, where n is the average number density, ∇p is the maximum pressure gradient in the cell, and η is the gas viscosity. The free molecular flux J_{FM} is roughly nv (neglecting geometrical factors), where v is the average atomic velocity. Insertion of typical numbers yields $J_V:J_{\text{FM}}:J_D \sim 10^{11}:10^5:1$, which indicates that wall recombination is limited by the diffusion rate, and viscous and free molecular flow may be neglected.

B. Experimental signal

A rigorous analysis of the polarization process for a given atom would require accounting for the changes in the populations of the individual hyperfine sublevels due to optical pumping, spin relaxation, and spin exchange. We use simple models of these processes, independent of the details of the hyperfine structure, in order to derive an approximate analytical solution. In this approximation, the time evolution of the electron-spin polarization $\langle S_z \rangle$ of each atom is described by

$$\begin{aligned} \frac{d\langle S_z \rangle}{dt} = & \left[\frac{d\langle S_z \rangle}{dt} \right]_{\text{optical pumping}} + \left[\frac{d\langle S_z \rangle}{dt} \right]_{\text{electron-spin relaxation}} \\ & + \left[\frac{d\langle S_z \rangle}{dt} \right]_{\text{Rb-H spin exchange}}. \end{aligned} \quad (8)$$

The first two terms are easily approximated as the optical-pumping rate varies linearly as $\langle S_z \rangle$, and electron-spin relaxation has nearly a simple exponential decay rate.⁷ The spin-exchange rate is a complicated function of $\langle S_z \rangle_{\text{Rb}}$ and $\langle S_z \rangle_{\text{H}}$, but the rate of change of the atomic polarization $d\langle F_z \rangle/dt$ is just proportional to the difference in $\langle S_z \rangle$ of the colliding atoms.¹⁸ We use the approximation $d\langle S_z \rangle/dt \approx d\langle F_z \rangle/dt$ in order to facilitate the analysis.

Combination of these simple models yields the two coupled equations

$$\begin{aligned} dS_{\text{Rb}}/dt \approx & \Gamma_{\text{op}}(\frac{1}{2} - S_{\text{Rb}}) - \gamma_{\text{Rb}} S_{\text{Rb}} \\ & + [\text{H}] \langle \sigma_{\text{Rb}v} \rangle (S_{\text{H}} - S_{\text{Rb}}), \end{aligned} \quad (9a)$$

$$dS_{\text{H}}/dt \approx -\gamma_{\text{H}} S_{\text{H}} + [\text{Rb}] \langle \sigma_{\text{H}v} \rangle (S_{\text{Rb}} - S_{\text{H}}), \quad (9b)$$

where $S_{\text{Rb}} \equiv \langle S_z \rangle_{\text{Rb}}$ and $S_{\text{H}} \equiv \langle S_z \rangle_{\text{H}}$, Γ_{op} is the optical-pumping rate in the unpolarized rubidium vapor, γ_{Rb} and γ_{H} are the rubidium and hydrogen electron-spin-relaxation rates, $\langle \sigma v \rangle$ is the average product of the Rb-H spin-exchange cross section and the relative speed of the colliding atoms. Since the electron transfers its spin to the nucleus through the hyperfine interaction, the atom must undergo several spin-exchange collisions be-

fore the electron remains polarized. Hence the effective spin-exchange cross section $\langle \sigma_{\text{Rb,H}} \rangle$ is equal to the real spin-exchange cross section $\langle \sigma \rangle$ divided by the "nuclear slowing-down factor" $(2I_{\text{Rb,H}} + 1)^2/2$, where I is the nuclear spin.⁷ All of these rates are effective values, averaged over the atomic hyperfine populations, the atomic velocity distributions, the spatial variation of the pumping light intensity, and the cell volume.

Because the hydrogen concentration is small, Eqs. (9a) and (9b) may be solved by expanding the polarizations in a power series in $[\text{H}]$ and solving iteratively. The discharge pulse causes total depolarization at the start of each half-cycle, so the initial conditions are $S_{\text{H}}(0) = S_{\text{Rb}}(0) = 0$. To zeroth order (assuming $[\text{H}] = 0$), the rubidium and hydrogen polarizations have the exact solutions

$${}^0S_{\text{Rb}}(t) = \frac{\frac{1}{2}\Gamma_{\text{op}}}{(\Gamma_{\text{op}} + \gamma_{\text{Rb}})} \left\{ 1 - \exp[-(\Gamma_{\text{op}} + \gamma_{\text{Rb}})t] \right\}, \quad (10a)$$

$${}^0S_{\text{H}}(t) = \frac{\frac{1}{2}\Gamma_{\text{op}}}{(\Gamma_{\text{op}} + \gamma_{\text{Rb}})} [\text{Rb}] \langle \sigma_{\text{H}\nu} \rangle \left\{ \frac{1}{(\gamma_{\text{H}} + [\text{Rb}] \langle \sigma_{\text{H}\nu} \rangle)} - \frac{\exp[-(\Gamma_{\text{op}} + \gamma_{\text{Rb}})t]}{(\gamma_{\text{H}} + [\text{Rb}] \langle \sigma_{\text{H}\nu} \rangle - \Gamma_{\text{op}} - \gamma_{\text{Rb}})} + \frac{(\Gamma_{\text{op}} + \gamma_{\text{Rb}}) \exp\{-(\gamma_{\text{H}} + [\text{Rb}] \langle \sigma_{\text{H}\nu} \rangle)t\}}{(\gamma_{\text{H}} + [\text{Rb}] \langle \sigma_{\text{H}\nu} \rangle)(\gamma_{\text{H}} + [\text{Rb}] \langle \sigma_{\text{H}\nu} \rangle - \Gamma_{\text{op}} - \gamma_{\text{Rb}})} \right\}. \quad (10b)$$

Equation (10a) describes the evolution of the rubidium polarization in the limit as $[\text{H}](t)$ goes to zero.

The first-order correction to the rubidium polarization is then

$$S_{\text{Rb}}(t) = {}^0S_{\text{Rb}}(t) + f(t)[\text{H}](t) \langle \sigma_{\text{Rb}\nu} \rangle, \quad (11)$$

where the hydrogen concentration decays exponentially due to wall recombination, as discussed previously.

$$[\text{H}](t) = [\text{H}]_0 \exp(-t/\tau). \quad (12)$$

When (11) is inserted in (9a), the remaining first-order terms are

$$df(t)/dt = f(t)(\tau^{-1} - \Gamma_{\text{op}} - \gamma_{\text{Rb}}) + {}^0S_{\text{H}}(t) - {}^0S_{\text{Rb}}(t). \quad (13)$$

This may be solved exactly for $f(t)$, and therefore for $S_{\text{Rb}}(t)$,

$$S_{\text{Rb}}(t) = \frac{\frac{1}{2}\Gamma_{\text{op}}}{(\Gamma_{\text{op}} + \gamma_{\text{Rb}})} \{ 1 - \exp[-(\Gamma_{\text{op}} + \gamma_{\text{Rb}})t] \} - \frac{\frac{1}{2}\Gamma_{\text{op}}(\gamma_{\text{H}} - \Gamma_{\text{op}} - \gamma_{\text{Rb}})[\text{H}]_0 \langle \sigma_{\text{Rb}\nu} \rangle}{(\Gamma_{\text{op}} + \gamma_{\text{Rb}})(\gamma_{\text{H}} + [\text{Rb}] \langle \sigma_{\text{H}\nu} \rangle - \Gamma_{\text{op}} - \gamma_{\text{Rb}})\tau^{-1}} \{ \exp[-(\Gamma_{\text{op}} + \gamma_{\text{Rb}} + \tau^{-1})t] - \exp[-(\Gamma_{\text{op}} + \gamma_{\text{Rb}})t] \} - \frac{\frac{1}{2}\Gamma_{\text{op}}[\text{Rb}] \langle \sigma_{\text{H}\nu} \rangle [\text{H}]_0 \langle \sigma_{\text{Rb}\nu} \rangle \{ \exp\{-(\gamma_{\text{H}} + [\text{Rb}] \langle \sigma_{\text{H}\nu} \rangle + \tau^{-1})t\} - \exp[-(\Gamma_{\text{op}} + \gamma_{\text{Rb}})t] \}}{(\gamma_{\text{H}} + [\text{Rb}] \langle \sigma_{\text{H}\nu} \rangle)(\gamma_{\text{H}} + [\text{Rb}] \langle \sigma_{\text{H}\nu} \rangle - \Gamma_{\text{op}} - \gamma_{\text{Rb}})(\gamma_{\text{H}} + [\text{Rb}] \langle \sigma_{\text{H}\nu} \rangle + \tau^{-1} - \Gamma_{\text{op}} - \gamma_{\text{Rb}})} - \frac{\frac{1}{2}\Gamma_{\text{op}}\gamma_{\text{H}}[\text{H}]_0 \langle \sigma_{\text{Rb}\nu} \rangle}{(\Gamma_{\text{op}} + \gamma_{\text{Rb}})(\gamma_{\text{H}} + [\text{Rb}] \langle \sigma_{\text{H}\nu} \rangle)(\Gamma_{\text{op}} + \gamma_{\text{Rb}} - \tau^{-1})} \{ \exp(-t/\tau) - \exp[-(\Gamma_{\text{op}} + \gamma_{\text{Rb}})t] \}. \quad (14)$$

Equation (14) describes the evolution of the rubidium polarization during the half-cycle in which the depolarizing rf is not turned on.

The evolution during the depolarization half-cycle is derived in the same way, except that $S_{\text{H}}(t)$ is zero (and $\gamma_{\text{H}} \rightarrow \infty$) during the short Zeeman pulse (applied at $t = t_0$) and evolves again afterward. The first-order solution during the Zeeman pulse of duration τ_z is

$$S_{\text{Rb}}(t) = \frac{\frac{1}{2}\Gamma_{\text{op}}}{(\Gamma_{\text{op}} + \gamma_{\text{Rb}})} \{ 1 - \exp[-(\Gamma_{\text{op}} + \gamma_{\text{Rb}})t] \} - \frac{\frac{1}{2}\Gamma_{\text{op}}[\text{H}]_0 \langle \sigma_{\text{Rb}\nu} \rangle}{(\Gamma_{\text{op}} + \gamma_{\text{Rb}})(\Gamma_{\text{op}} + \gamma_{\text{Rb}} - \tau^{-1})} \{ \exp(-t/\tau) - \exp[-(\Gamma_{\text{op}} + \gamma_{\text{Rb}})(t - t_0)] \exp(-t_0/\tau) \} - \frac{\frac{1}{2}\Gamma_{\text{op}}[\text{H}]_0 \langle \sigma_{\text{Rb}\nu} \rangle}{(\Gamma_{\text{op}} + \gamma_{\text{Rb}})\tau^{-1}} \{ \exp[-(\Gamma_{\text{op}} + \gamma_{\text{Rb}} + \tau^{-1})t] - \exp[-(\Gamma_{\text{op}} + \gamma_{\text{Rb}})t] \exp(-t_0/\tau) \} + \frac{\frac{1}{2}\Gamma_{\text{op}}\gamma_{\text{H}}[\text{H}]_0 \langle \sigma_{\text{Rb}\nu} \rangle \exp[-(\Gamma_{\text{op}} + \gamma_{\text{Rb}})t]}{(\Gamma_{\text{op}} + \gamma_{\text{Rb}})(\gamma_{\text{H}} + [\text{Rb}] \langle \sigma_{\text{H}\nu} \rangle)(\Gamma_{\text{op}} + \gamma_{\text{Rb}} - \tau^{-1})} [1 - \exp(\Gamma_{\text{op}} + \gamma_{\text{Rb}} + \tau^{-1})t_0] + \frac{\frac{1}{2}\Gamma_{\text{op}}[\text{Rb}] \langle \sigma_{\text{H}\nu} \rangle [\text{H}]_0 \langle \sigma_{\text{Rb}\nu} \rangle \exp[-(\Gamma_{\text{op}} + \gamma_{\text{Rb}})t] \{ 1 - \exp\{-(\gamma_{\text{H}} + [\text{Rb}] \langle \sigma_{\text{H}\nu} \rangle + \tau^{-1} - \Gamma_{\text{op}} - \gamma_{\text{Rb}})t_0\} \}}{(\gamma_{\text{H}} + [\text{Rb}] \langle \sigma_{\text{H}\nu} \rangle)(\gamma_{\text{H}} + [\text{Rb}] \langle \sigma_{\text{H}\nu} \rangle - \Gamma_{\text{op}} - \gamma_{\text{Rb}})(\gamma_{\text{H}} + [\text{Rb}] \langle \sigma_{\text{H}\nu} \rangle + \tau^{-1} - \Gamma_{\text{op}} - \gamma_{\text{Rb}})} + \frac{\frac{1}{2}\Gamma_{\text{op}}(\gamma_{\text{H}} - \Gamma_{\text{op}} - \gamma_{\text{Rb}})[\text{H}]_0 \langle \sigma_{\text{Rb}\nu} \rangle \exp[-(\Gamma_{\text{op}} + \gamma_{\text{Rb}})t]}{(\Gamma_{\text{op}} + \gamma_{\text{Rb}})(\gamma_{\text{H}} + [\text{Rb}] \langle \sigma_{\text{H}\nu} \rangle - \Gamma_{\text{op}} - \gamma_{\text{Rb}})\tau^{-1}} [1 - \exp(-t_0/\tau)] \quad (15a)$$

and the solution after the pulse ends ($t > t_1 \equiv t_0 + \tau_z$) is

$$\begin{aligned}
S_{\text{Rb}}(t) = & \frac{\frac{1}{2}\Gamma_{\text{op}}}{(\Gamma_{\text{op}} + \gamma_{\text{Rb}})} \{1 - \exp[-(\Gamma_{\text{op}} + \gamma_{\text{Rb}})t]\} \\
& - \frac{\frac{1}{2}\Gamma_{\text{op}}\gamma_{\text{H}}[\text{H}]_0 \langle \sigma_{\text{Rb}\nu} \rangle \exp[-(\Gamma_{\text{op}} + \gamma_{\text{Rb}})t]}{(\Gamma_{\text{op}} + \gamma_{\text{Rb}})(\gamma_{\text{H}} + [\text{Rb}]\langle \sigma_{\text{H}\nu} \rangle)(\Gamma_{\text{op}} + \gamma_{\text{Rb}} - \tau^{-1})} \{ \exp(-t/\tau) - \exp[-(\Gamma_{\text{op}} + \gamma_{\text{Rb}})(t - t_1)] \exp(-t_1/\tau) \} \\
& - \frac{\frac{1}{2}\Gamma_{\text{op}}(\gamma_{\text{H}} - \Gamma_{\text{op}} - \gamma_{\text{Rb}})[\text{H}]_0 \langle \sigma_{\text{Rb}\nu} \rangle}{(\Gamma_{\text{op}} + \gamma_{\text{Rb}})(\gamma_{\text{H}} + [\text{Rb}]\langle \sigma_{\text{H}\nu} \rangle - \Gamma_{\text{op}} - \gamma_{\text{Rb}})\tau^{-1}} \\
& \times \{ \exp[-(\Gamma_{\text{op}} + \gamma_{\text{Rb}} + \tau^{-1})t] - \exp[-(\Gamma_{\text{op}} + \gamma_{\text{Rb}})t] \exp(-t_1/\tau) \} \\
& - \frac{\frac{1}{2}\Gamma_{\text{op}}[\text{Rb}]\langle \sigma_{\text{H}\nu} \rangle [\text{H}]_0 \langle \sigma_{\text{Rb}\nu} \rangle}{(\Gamma_{\text{op}} + \gamma_{\text{Rb}})(\gamma_{\text{H}} + [\text{Rb}]\langle \sigma_{\text{H}\nu} \rangle + \tau^{-1} - \Gamma_{\text{op}} - \gamma_{\text{Rb}})} \left\{ \frac{\exp[-(\Gamma_{\text{op}} + \gamma_{\text{Rb}} + \tau^{-1})t_1]}{(\gamma_{\text{H}} + [\text{Rb}]\langle \sigma_{\text{H}\nu} \rangle - \Gamma_{\text{op}} - \gamma_{\text{Rb}})} - \frac{\exp(-t_1/\tau)}{(\gamma_{\text{H}} + [\text{Rb}]\langle \sigma_{\text{H}\nu} \rangle)} \right\} \\
& \times \{ \exp\{-(\gamma_{\text{H}} + [\text{Rb}]\langle \sigma_{\text{H}\nu} \rangle + \tau^{-1})(t - t_1)\} - \exp[-(\Gamma_{\text{op}} + \gamma_{\text{Rb}})(t - t_1)] \} \\
& + \frac{\frac{1}{2}\Gamma_{\text{op}}\gamma_{\text{H}}[\text{H}]_0 \langle \sigma_{\text{Rb}\nu} \rangle \exp[-(\Gamma_{\text{op}} + \gamma_{\text{Rb}})t]}{(\Gamma_{\text{op}} + \gamma_{\text{Rb}})(\gamma_{\text{H}} + [\text{Rb}]\langle \sigma_{\text{H}\nu} \rangle)(\Gamma_{\text{op}} + \gamma_{\text{Rb}} - \tau^{-1})} [1 - \exp(\Gamma_{\text{op}} + \gamma_{\text{Rb}} + \tau^{-1})t_0] \\
& + \frac{\frac{1}{2}\Gamma_{\text{op}}[\text{Rb}]\langle \sigma_{\text{H}\nu} \rangle [\text{H}]_0 \langle \sigma_{\text{Rb}\nu} \rangle \exp[-(\Gamma_{\text{op}} + \gamma_{\text{Rb}})t] (1 - \exp\{-(\gamma_{\text{H}} + [\text{Rb}]\langle \sigma_{\text{H}\nu} \rangle + \tau^{-1} - \Gamma_{\text{op}} - \gamma_{\text{Rb}})t_0\})}{(\gamma_{\text{H}} + [\text{Rb}]\langle \sigma_{\text{H}\nu} \rangle)(\gamma_{\text{H}} + [\text{Rb}]\langle \sigma_{\text{H}\nu} \rangle - \Gamma_{\text{op}} - \gamma_{\text{Rb}})(\gamma_{\text{H}} + [\text{Rb}]\langle \sigma_{\text{H}\nu} \rangle + \tau^{-1} - \Gamma_{\text{op}} - \gamma_{\text{Rb}})} \\
& + \frac{\frac{1}{2}\Gamma_{\text{op}}(\gamma_{\text{H}} - \Gamma_{\text{op}} - \gamma_{\text{Rb}})[\text{H}]_0 \langle \sigma_{\text{Rb}\nu} \rangle \exp[-(\Gamma_{\text{op}} + \gamma_{\text{Rb}})t]}{(\Gamma_{\text{op}} + \gamma_{\text{Rb}})(\gamma_{\text{H}} + [\text{Rb}]\langle \sigma_{\text{H}\nu} \rangle - \Gamma_{\text{op}} - \gamma_{\text{Rb}})\tau^{-1}} [1 - \exp(-t_0/\tau)] \\
& + \frac{\frac{1}{2}\Gamma_{\text{op}}[\text{H}]_0 \langle \sigma_{\text{Rb}\nu} \rangle \exp[-(\Gamma_{\text{op}} + \gamma_{\text{Rb}})t]}{(\Gamma_{\text{op}} + \gamma_{\text{Rb}})(\Gamma_{\text{op}} + \gamma_{\text{Rb}} - \tau^{-1})} [\exp(\Gamma_{\text{op}} + \gamma_{\text{Rb}} + \tau^{-1})t_0 - \exp(\Gamma_{\text{op}} + \gamma_{\text{Rb}} + \tau^{-1})t_1] \\
& + \frac{\frac{1}{2}\Gamma_{\text{op}}[\text{H}]_0 \langle \sigma_{\text{Rb}\nu} \rangle \exp[-(\Gamma_{\text{op}} + \gamma_{\text{Rb}})t]}{(\Gamma_{\text{op}} + \gamma_{\text{Rb}})\tau^{-1}} [\exp(-t_0/\tau) - \exp(-t_1/\tau)] . \tag{15b}
\end{aligned}$$

In this experiment the optical-pumping light source is also used as a probe for transmission monitoring of the rubidium polarization. The intensity I transmitted through a cell of optical path length L is

$$I = I_0 \exp(-[\text{Rb}]\sigma L) , \tag{16}$$

where I_0 is the intensity of light entering the cell and $\sigma = \sigma_0(1 - 2S_{\text{Rb}})$ is the absorption cross section (σ_0 is the absorption cross section for unpolarized light). The lock-in signal is proportional to the difference in the light transmitted during consecutive half-cycles, averaged over many cycles. If $\Delta S_{\text{Rb}} \equiv S_{\text{Rb}}(\text{rf off}) - S_{\text{Rb}}(\text{rf on})$ is small, then the change in light transmission ΔI is proportional to ΔS_{Rb} ,

$$\Delta I = 2[\text{Rb}]\sigma_0 L I \Delta S_{\text{Rb}} . \tag{17}$$

The hydrogen signal $A_{\text{H}}(t_0)$ is found by integrating ΔI over the time intervals during and after the depolarizing pulse,

$$A_{\text{H}}(t_0) = \frac{\eta}{\tau_c/2} \int_{t_0}^{\tau_c/2} \Delta S_{\text{Rb}}(t) dt . \tag{18}$$

The signal is normalized by the length $\tau_c/2$ of the half-cycle and the factor η represents the efficiency of the detection electronics and the factor $2[\text{Rb}]\sigma_0 L I$. Upon integration, the hydrogen signal becomes the following expression (to first order in $[\text{H}]$):

$A_H(t_0)$

$$\begin{aligned}
&= \eta \frac{(\Gamma_{op}/\tau_c)[\text{Rb}]\langle\sigma_{H\nu}\rangle[\text{H}]_0\langle\sigma_{\text{Rb}\nu}\rangle \exp(-t_0/\tau)}{(\Gamma_{op}+\gamma_{\text{Rb}})(\gamma_H+[\text{Rb}]\langle\sigma_{H\nu}\rangle)(\Gamma_{op}+\gamma_{\text{Rb}}-\tau^{-1})\tau^{-1}} [1-\exp(-\tau_z/\tau)] \\
&+ \eta \frac{(\Gamma_{op}/\tau_c)[\text{Rb}]\langle\sigma_{H\nu}\rangle[\text{H}]_0\langle\sigma_{\text{Rb}\nu}\rangle \exp[-(\Gamma_{op}+\gamma_{\text{Rb}}+\tau^{-1})t_0]}{(\Gamma_{op}+\gamma_{\text{Rb}})(\gamma_H+[\text{Rb}]\langle\sigma_{H\nu}\rangle-\Gamma_{op}-\gamma_{\text{Rb}})(\Gamma_{op}+\gamma_{\text{Rb}}+\tau^{-1})\tau^{-1}} \{1-\exp[-(\Gamma_{op}+\gamma_{\text{Rb}}+\tau^{-1})\tau_z]\} \\
&- \eta \frac{(\Gamma_{op}/\tau_c)[\text{Rb}]\langle\sigma_{H\nu}\rangle[\text{H}]_0\langle\sigma_{\text{Rb}\nu}\rangle \exp(-t_0/\tau)}{(\Gamma_{op}+\gamma_{\text{Rb}})^2(\gamma_H+[\text{Rb}]\langle\sigma_{H\nu}\rangle)(\Gamma_{op}+\gamma_{\text{Rb}}-\tau^{-1})} \{1-\exp[-(\Gamma_{op}+\gamma_{\text{Rb}})(\tau_c/2-t_0)]\} \\
&- \eta \frac{(\Gamma_{op}/\tau_c)[\text{Rb}]\langle\sigma_{H\nu}\rangle[\text{H}]_0\langle\sigma_{\text{Rb}\nu}\rangle \exp[-(\Gamma_{op}+\gamma_{\text{Rb}}+\tau^{-1})t_0]}{(\Gamma_{op}+\gamma_{\text{Rb}})^2(\gamma_H+[\text{Rb}]\langle\sigma_{H\nu}\rangle-\Gamma_{op}-\gamma_{\text{Rb}})\tau^{-1}} \{1-\exp[-(\Gamma_{op}+\gamma_{\text{Rb}})(\tau_c/2-t_0)]\} \\
&+ \eta \frac{(\Gamma_{op}/\tau_c)[\text{Rb}]\langle\sigma_{H\nu}\rangle[\text{H}]_0\langle\sigma_{\text{Rb}\nu}\rangle \exp\{-(\gamma_H+[\text{Rb}]\langle\sigma_{H\nu}\rangle+\tau^{-1})t_0\} \{1-\exp[-(\Gamma_{op}+\gamma_{\text{Rb}})(\tau_c/2-t_0)]\}}{(\Gamma_{op}+\gamma_{\text{Rb}})(\gamma_H+[\text{Rb}]\langle\sigma_{H\nu}\rangle)(\gamma_H+[\text{Rb}]\langle\sigma_{H\nu}\rangle-\Gamma_{op}-\gamma_{\text{Rb}})(\gamma_H+[\text{Rb}]\langle\sigma_{H\nu}\rangle+\tau^{-1}-\Gamma_{op}-\gamma_{\text{Rb}})} \\
&- \eta \frac{(\Gamma_{op}/\tau_c)[\text{Rb}]\langle\sigma_{H\nu}\rangle[\text{H}]_0\langle\sigma_{\text{Rb}\nu}\rangle \exp\{-(\gamma_H+[\text{Rb}]\langle\sigma_{H\nu}\rangle+\tau^{-1})t_0\}}{(\gamma_H+[\text{Rb}]\langle\sigma_{H\nu}\rangle)(\gamma_H+[\text{Rb}]\langle\sigma_{H\nu}\rangle-\Gamma_{op}-\gamma_{\text{Rb}})(\gamma_H+[\text{Rb}]\langle\sigma_{H\nu}\rangle+\tau^{-1}-\Gamma_{op}-\gamma_{\text{Rb}})(\gamma_H+[\text{Rb}]\langle\sigma_{H\nu}\rangle+\tau^{-1})} \\
&\quad \times (1-\exp\{-(\gamma_H+[\text{Rb}]\langle\sigma_{H\nu}\rangle+\tau^{-1})(\tau_c/2-t_0)\}) \\
&- \eta \frac{(\Gamma_{op}/\tau_c)[\text{Rb}]\langle\sigma_{H\nu}\rangle[\text{H}]_0\langle\sigma_{\text{Rb}\nu}\rangle \exp(-t_1/\tau) (1-\exp\{-(\gamma_H+[\text{Rb}]\langle\sigma_{H\nu}\rangle+\tau^{-1})(\tau_c/2-t_1)\})}{(\Gamma_{op}+\gamma_{\text{Rb}})(\gamma_H+[\text{Rb}]\langle\sigma_{H\nu}\rangle)(\gamma_H+[\text{Rb}]\langle\sigma_{H\nu}\rangle+\tau^{-1}-\Gamma_{op}-\gamma_{\text{Rb}})(\gamma_H+[\text{Rb}]\langle\sigma_{H\nu}\rangle+\tau^{-1})} \\
&+ \eta \frac{(\Gamma_{op}/\tau_c)[\text{Rb}]\langle\sigma_{H\nu}\rangle[\text{H}]_0\langle\sigma_{\text{Rb}\nu}\rangle \exp[-(\Gamma_{op}+\gamma_{\text{Rb}}+\tau^{-1})t_1] (1-\exp\{-(\gamma_H+[\text{Rb}]\langle\sigma_{H\nu}\rangle+\tau^{-1})(\tau_c/2-t_1)\})}{(\Gamma_{op}+\gamma_{\text{Rb}})(\gamma_H+[\text{Rb}]\langle\sigma_{H\nu}\rangle-\Gamma_{op}-\gamma_{\text{Rb}})(\gamma_H+[\text{Rb}]\langle\sigma_{H\nu}\rangle+\tau^{-1}-\Gamma_{op}-\gamma_{\text{Rb}})(\gamma_H+[\text{Rb}]\langle\sigma_{H\nu}\rangle+\tau^{-1})} \\
&+ \eta \frac{(\Gamma_{op}/\tau_c)[\text{Rb}]\langle\sigma_{H\nu}\rangle[\text{H}]_0\langle\sigma_{\text{Rb}\nu}\rangle \exp(-t_1/\tau) \{1-\exp[-(\Gamma_{op}+\gamma_{\text{Rb}})(\tau_c/2-t_1)]\}}{(\Gamma_{op}+\gamma_{\text{Rb}})^2(\gamma_H+[\text{Rb}]\langle\sigma_{H\nu}\rangle+\tau^{-1}-\Gamma_{op}-\gamma_{\text{Rb}})(\Gamma_{op}+\gamma_{\text{Rb}}-\tau^{-1})} \\
&+ \eta \frac{(\Gamma_{op}/\tau_c)[\text{Rb}]\langle\sigma_{H\nu}\rangle[\text{H}]_0\langle\sigma_{\text{Rb}\nu}\rangle \exp[-(\Gamma_{op}+\gamma_{\text{Rb}}+\tau^{-1})t_1]}{(\Gamma_{op}+\gamma_{\text{Rb}})^2(\gamma_H+[\text{Rb}]\langle\sigma_{H\nu}\rangle+\tau^{-1}-\Gamma_{op}-\gamma_{\text{Rb}})\tau^{-1}} \{1-\exp[-(\Gamma_{op}+\gamma_{\text{Rb}})(\tau_c/2-t_1)]\}. \quad (19)
\end{aligned}$$

The typical values of the rates and time constants used in this experiment are $\Gamma_{op} \sim 100 \text{ sec}^{-1}$, $\gamma_{\text{Rb}} \sim 100 \text{ sec}^{-1}$, $\gamma_H \sim 600 \text{ sec}^{-1}$, $[\text{Rb}] \sim 10^{11} \text{ cm}^{-3}$, $[\text{H}]_0 \sim 10^{12} \text{ cm}^{-3}$, $\langle\sigma_{\nu}\rangle \sim 10^{-9} \text{ cm}^3 \text{ sec}^{-1}$, $\tau^{-1} \sim 100 \text{ sec}^{-1}$, $\tau_z = 2 \text{ msec}$, and $\tau_c/2 \sim 100 \text{ msec}$. These values allow Eq. (19) to be simplified by the approximation that all exponential terms besides $\exp(-t_0/\tau)$ and $\exp(-t_1/\tau)$ are negligible compared to these two if t_0 is large ($\gtrsim 25 \text{ msec}$). This includes all but the slowest diffusion mode ($m=1$) of Eq. (6), as previously stated. With this approximation, the signal amplitude after a long delay t_0 reduces to

$$A_H(t_0) = \eta \exp(-t_0/\tau) \frac{(\Gamma_{op}/\tau_c)[\text{H}]_0\langle\sigma_{\text{Rb}\nu}\rangle[\text{Rb}]\langle\sigma_{H\nu}\rangle}{(\Gamma_{op}+\gamma_{\text{Rb}})^2(\gamma_H+[\text{Rb}]\langle\sigma_{H\nu}\rangle+\tau^{-1})} \left[\frac{1}{(\gamma_H+[\text{Rb}]\langle\sigma_{H\nu}\rangle)} + \frac{1-\exp(-\tau_z/\tau)}{\tau^{-1}} \right]. \quad (20)$$

Equation (20) shows that to first order in $[\text{H}]$, the time dependence of the hydrogen signal after allowing sufficient time for the polarizations to become established is an exponential with decay rate τ^{-1} due to diffusion of hydrogen atoms to the cell walls. In Figure 4 the single exponential approximation of Eq. (20) is compared graphically to an exact numerical solution of Eqs. (9a) and (9b) using the typical parameters listed above, showing the validity of this approximation at large delay times.

It can similarly be shown⁹ that if the depolarizing pulse is applied at the rubidium Zeeman frequency, the rubidium signal is (for large t_0)

$$A_{\text{Rb}}(t_0) = \eta \frac{(\Gamma_{op}/\tau_c)}{(\Gamma_{op}+\gamma_{\text{Rb}})^2}. \quad (20a)$$

The ratio of the hydrogen and rubidium signals for large t_0 is thus

$$\begin{aligned}
\frac{A_H}{A_{\text{Rb}}} &= \frac{[\text{Rb}]\langle\sigma_{H\nu}\rangle[\text{H}]_0\langle\sigma_{\text{Rb}\nu}\rangle \exp(-t_0/\tau)}{(\gamma_H+[\text{Rb}]\langle\sigma_{H\nu}\rangle)(\gamma_H+[\text{Rb}]\langle\sigma_{H\nu}\rangle+\tau^{-1})} \\
&\quad \times \left[1 + \frac{(\gamma_H+[\text{Rb}]\langle\sigma_{H\nu}\rangle)}{\tau^{-1}} [1-\exp(-\tau_z/\tau)] \right]. \quad (20b)
\end{aligned}$$

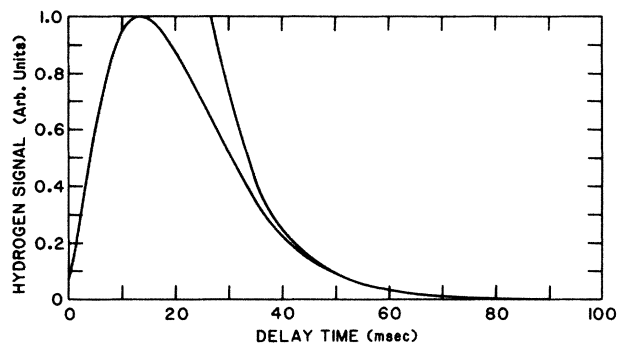


FIG. 4. Numerical calculation of the hydrogen signal compared to our single exponential approximation [Eq. (20)]. The single exponential approximation becomes valid at large delay times. The rates, number densities, and pulse widths used in the calculation are those listed in the text.

The [Rb] dependence of this signal ratio may be used to determine the hydrogen spin-relaxation rate γ_H , the spin-exchange rate $\langle\sigma\nu\rangle$, and the initial hydrogen concentration $[H]_0$ produced by the discharge.

IV. DATA REDUCTION

Several experimental variables were set separately for each cell in order to maximize the hydrogen signal-to-noise ratio of each measurement. These include the rf power and tuning of the discharge coil, the lengths of the master clock and discharge pulses, and the temperature of the cell. A typical temperature dependence of the peak hydrogen signal is shown in Fig. 5. The temperature of the cell determines the rubidium density. At low rubidium density, the spin-exchange rate is too low to strongly couple the rubidium and hydrogen spins. At high rubidium density, the transmission is reduced due to increased light absorption. The optimum alkali-metal concentration could also be maintained at other temperatures either by cooling the rubidium in a separate reservoir while the rest of the cell is heated or by using another alkali-metal (K,Cs) with a different vapor-

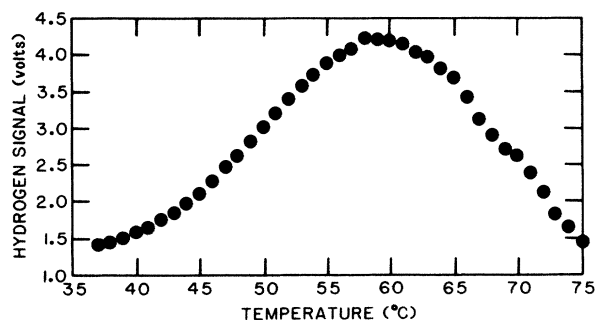


FIG. 5. Typical plot of the observed hydrogen signal as a function of the cell temperature. At low temperatures, the rubidium density is so low that spin exchange is insufficient to polarize the hydrogen atoms before they diffuse to the cell wall and recombine. At high temperatures, the rubidium density is high enough to reduce light transmission through the cell.

pressure curve. This would allow the measurement of D_0 over an extended temperature range.

In order to investigate possible systematic errors, the cell temperature and longitudinal magnetic field were varied. Data were taken on one cell at temperatures from 40 to 70°C. In this temperature range, the rubidium concentration varies by an order of magnitude,¹³ yet the decay rate was not observed to change significantly with rubidium concentration (or to deviate from the expected temperature dependence, which will be discussed later). There was also no significant difference in the decay rate when the longitudinal magnetic field was increased from 0.59 to 1.38 G. Hence the temperatures and magnetic fields used in this experiment do not seem to have introduced any significant errors into these results.

The decay rate for an individual hydrogen signal (as in Fig. 3) was determined by a least-squares fit of the signal to an exponential-decay function. As previously indicated, the exponential decay becomes a good approximation only well after the peak of the signal, by which time the faster diffusion modes of Eq. (6) and the faster exponentials left out of Eq. (20) may be neglected. Therefore, the curve fit was begun at the point at which the hydrogen signal had decayed to about 30% of its peak value. Variations in the starting point of the curve fit were not found to significantly affect the calculated decay rate.

In Fig. 6 the measured-signal decay rate τ_{H-He}^{-1} is plotted as a function of the cell radius and helium pressure at an oven temperature of about 60°C. The decay rate plotted for each of the 13 cells is the average of four individual measurements taken for that cell (with the correction for $\tau_{H-H_2}^{-1}$), and the vertical error bars represent the standard deviation of the mean of these measurements. The helium pressure was determined by correction of the fill pressure from room temperature to the oven temperature. From these data, which were analyzed by a least-squares fit to a straight line through the origin, the diffusion constant of atomic hydrogen in heli-

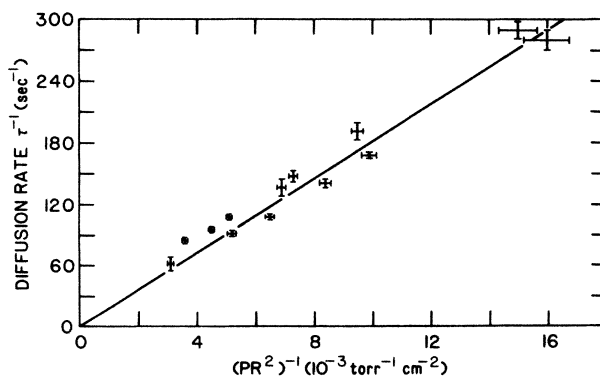


FIG. 6. Decay rate of the hydrogen signal as a function of the cell radius and helium partial pressure. The straight line corresponds to the measured diffusion constant at 60°C, $D_0 = 2.42(7) \text{ cm}^2 \text{ sec}^{-1}$. The vertical error bars are the statistical error in the decay rate (standard deviation of the mean). The horizontal error bars represent the uncertainty in the cell radii.

um at 60°C and 760 torr was determined to be 2.42(7) $\text{cm}^2 \text{sec}^{-1}$. This value is represented by the straight line through the points in Fig. 6.

In addition to the statistical error, the systematic errors due to temperature fluctuations and uncertainties in the gas pressure and the cell radius must be estimated. Typical temperature fluctuations were about ± 1.5 K around ~ 333 K, which implies an uncertainty of about 1%. The uncertainty in gas pressure was less than one part in 10^3 . The finite and nonuniform thickness of the cell walls and the fact that the cells were not perfectly spherical contributed to an estimated uncertainty of 0.5 mm in the cell diameter, an error of 1–3%. Adding the systematic errors in quadrature, the errors in temperature and pressure are negligible compared to the uncertainties in the cell radii, which are shown as the horizontal error bars in Fig. 6.

V. DISCUSSION

Because the slope of the real interatomic potential is finite, the temperature dependence of the diffusion constant deviates from the classical $T^{3/2}$ dependence expected for a billiard-ball interatomic potential. In the temperature range of this experiment, the temperature dependence of D_0 has been calculated to be about $T^{1.77}$ (as may be seen in Table I, which is discussed below). Hence the result of this experiment may be scaled to

TABLE I. Diffusion constants calculated from the cited H-He interatomic potentials. The stated errors for Refs. 19–24 and 26 are the uncertainties in the numerical quadratures (Ref. 25); the uncertainties in the potentials were not taken into account. The errors in the experimental measurements (Refs. 5 and 14) are the stated experimental uncertainties. Numbers in square brackets are the experimental measurements extrapolated into the other column, assuming that the diffusion constant varies with temperature as $T^{1.77}$. The exponent 1.77(2) represents the average temperature dependence of the calculations for the potentials of Refs. 19–23.

Theoretical potentials	$D_0(0^\circ\text{C})$	$D_0(60^\circ\text{C})$
Mason <i>et al.</i> ^a	1.655(4)	2.346(6)
Das and Ray ^b	1.673(4)	2.385(6)
Miller and Schaefer ^c	1.684(5)	2.402(7)
Davison and Liew ^d	1.757(5)	2.491(7)
Das <i>et al.</i> ^e	1.844(4)	2.610(6)
Jochemsen <i>et al.</i> ^f	1.970(5)	2.750(7)
Experimental potential Gengenbach <i>et al.</i> ^g	1.978(5)	2.756(7)
Experimental measurements		
This work	[1.70(5)]	2.42(7)
Kartoshkin <i>et al.</i> ^h	1.86(19)	[2.64(26)]
Khouw <i>et al.</i> ⁱ	2.38	[3.38]

^aReference 19.

^bReference 20.

^cReference 21.

^dReference 22.

^eReference 23.

^fReference 24.

^gReference 26.

^hReference 5.

ⁱReference 14.

other temperatures, yielding $D_0(273 \text{ K}) = 1.70(5) \text{ cm}^2 \text{sec}^{-1}$. Figure 7 compares the result of this experiment to those of Khouw *et al.*,¹⁴ who found $D_0(273 \text{ K}) = 2.38 \text{ cm}^2 \text{sec}^{-1}$ using a catalytic sink technique, and Kartoshkin *et al.*,⁵ who found $D_0(273^\circ \text{ K}) = 1.86(19) \text{ cm}^2 \text{sec}^{-1}$ by analysis of the magnetic resonance linewidths of Zeeman transitions in hydrogen atoms. The result of this report is much lower than that of Khouw *et al.* and somewhat lower than that of Kartoshkin *et al.* However, it is possible that both of these previous experiments involved systematic errors which led to overestimation of the diffusion constant. In Kartoshkin *et al.*, the hydrogen line broadening was assumed to be entirely due to diffusion, yet other broadening processes could have contributed to the linewidth and therefore enhanced the calculated diffusion constant. In Khouw *et al.* the diffusion constant is a function of the concentration and flow velocity of gas in a cylindrical tube. Their analysis accounted for the possibility of small radial concentration gradients in the tube but did not account for any radial velocity dependence, instead assuming a uniform flow at the velocity measured in the center of the tube, where the flow rate is greatest. The diffusion constant calculated using this maximum velocity would be significantly higher than that calculated using a velocity averaged over the radius of the tube.

Our measured diffusion constant may be used to gain information about the H-He interaction potential. Because all transport phenomena arise due to deviation from the equilibrium molecular velocity distribution, the diffusion constant is found by solving the Boltzmann equation for the nonequilibrium distribution. Diffusion is related to the momentum transferred during binary collisions, which to a first approximation are assumed to be elastic. In this approximation (Chapman-Enskog theory¹⁷), the diffusion constant D is given by

$$D = \frac{3}{16} \left[\frac{2\pi kT}{\mu} \right]^{1/2} \frac{1}{n\Omega_{11}(T)}, \quad (21)$$

where μ is the reduced mass of the binary system, n is the total atomic number density, and Ω_{11} is a collision

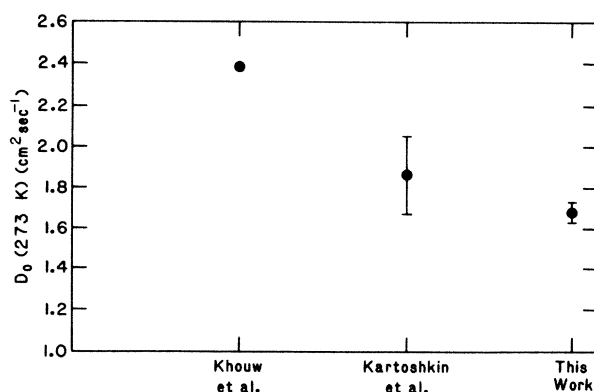


FIG. 7. Graphic comparison of experimental results, obtained in this experiment and those of Refs. 5 and 14 for $D_0(\text{H-He})$ at 273 K.

integral

$$\Omega_{11} = \frac{1}{2} \int_0^\infty e^{-x^2} \sigma(E) dx, \quad (22)$$

where

$$\sigma(E) = 2\pi \int_0^\infty b db (1 - \cos \vartheta) \quad (23)$$

and

$$\vartheta(E, b) = \pi - 2b \int_{r_m}^\infty \frac{r^{-2} dr}{[1 - V(r)/E - b^2/r^2]^{1/2}}. \quad (24)$$

In these expressions, $\sigma(E)$ is the momentum-transfer cross section, where $x = E/kT$ is the ratio of the initial kinetic energy of the colliding molecules to the temperature, and $\vartheta(E, b)$ is the classical scattering angle for a collision at initial kinetic energy E , impact parameter b , and classical turning point r_m . Hence it is possible to evaluate Ω_{11} and D_0 using the H-He interatomic potential.

Theoretical potential calculations use combinations of modified Hartree-Fock atomic orbital configurations to construct the interatomic potential.¹⁹⁻²⁴ These numerical calculations may be fit to various semiempirical analytical forms (usually matching a short-range exponential repulsion due to electronic screening and a long-range multipolar attraction) in order to evaluate the collision integrals by standard techniques of numerical integration.²⁵

We have evaluated the diffusion constants for these theoretical potentials and also for one experimentally determined potential.²⁶ These results are listed in Table I. It was found that the calculated diffusion constants were most sensitive to the repulsive part of the interatomic potential at energies on the order of the temperature kT . While most of these theoretical calculations are within 10% of our experimental result, those of Jochemsen *et al.*²⁴ and Gengenbach *et al.*²⁶ are sufficiently far off to suggest that their form of the repulsive part of the H-He interaction potential is inaccurate. In fact, the repulsive part of the potential of Jochemsen *et al.* is based on the experimental results of Gengenbach *et al.* These results come from scattering experiments at beam energies of a few hundred meV, which is an order of magnitude larger than the energy equivalent of 333 K. Hence the disagreement between our measured diffusion constant and that calculated from the analytical potential of Gengenbach *et al.* implies that the scattering cross section is significantly different from the cross section pre-

dicted by their extrapolation to lower beam energies.

Our calculations of the diffusion constants assumed a classical interaction model, ignoring quantum-mechanical corrections to the collision integrals. Quantum and classical calculations of the collision integral Ω_{11} were performed using an *ab initio* potential suggested by Scoles.²⁷ The ratio $\Omega_{11}(\text{classical})/\Omega_{11}(\text{quantum})$ was found to be about 1.0065, which implies that the quantum-mechanical enhancement of $D_0(\text{H-He})$ is less than 1%. Improvements in the accuracy of this technique could be used to compare quantum-mechanical effects on the H-He and D-He interactions by measurement of $D_0(\text{H-He})$ and $D_0(\text{D-He})$ in cells containing helium, hydrogen, and deuterium.

VI. SUMMARY

The diffusion constant of atomic hydrogen in helium gas was measured using an optical-pumping-spin-exchange technique. The result obtained in this experiment, $D_0(60^\circ\text{C}) = 2.42(7) \text{ cm}^2 \text{ sec}^{-1}$, is in good agreement with most theoretical calculations and is significantly more accurate than the results of previous experiments.

Because of the accuracy of this method, the measured diffusion constant may be used to obtain information about the interatomic potential energy. Such quantities as the steepness of the repulsive potential at energies comparable to kT and the location of the zero crossing could be determined accurately by measuring the diffusion constant over a wide range of temperatures.

The diffusion of atomic species such as hydrogen, deuterium, and nitrogen (or electrons), which can be difficult or impractical to measure by conventional methods, may be investigated using the present technique. This method may be used to compare the diffusion of isotopes with different nuclear spin, such as hydrogen and deuterium, in the same volume.

ACKNOWLEDGMENTS

The authors are especially grateful to R. A. Aziz for performing the *ab initio* quantum and classical collision integral calculations, and also thank G. Scoles for valuable discussions. This work was supported by the U.S. Department of Energy under Contract No. DE-AC02-76CHO3973 and by the U.S. Air Force Office of Scientific Research under Grant No. AFOSR-81-0104-C.

¹D. E. Post, D. B. Heifetz, and M. Petravic, *J. Nucl. Mater.* **111-112**, 383 (1982).

²W. N. Hardy and M. Morrow, *J. Phys. (Paris) Colloq.* **42**, C8-171 (1981).

³W. Kolos and L. Wolniewicz, *Chem. Phys. Lett.* **24**, 457 (1974).

⁴R. D. Present, *Kinetic Theory of Gases* (McGraw-Hill, New York, 1958).

⁵V. A. Kartoshkin, G. V. Klementev, and V. D. Melnikov, *Op.*

Spektrosk. **55**, 606 (1983) [*Opt. Spectrosc. (USSR)* **55**, 358 (1983)].

⁶E. I. Asinovskii, R. K. Amirov, L. M. Vasilyak, and V. V. Markovets, *Teplofiz. Vys. Temp.* **17**, 912 (1979) [*High Temp. (USSR)* **17**, 755 (1979)].

⁷W. Happer, *Rev. Mod. Phys.* **44**, 169 (1972).

⁸L. W. Anderson, F. M. Pipkin, and J. C. Baird, *Phys. Rev. Lett.* **4**, 69 (1960).

⁹R. J. Knize and J. L. Cecchi, *Phys. Rev. A* **33**, 3595 (1986).

- ¹⁰W. N. Hardy, M. Morrow, R. Jochemsen, B. W. Statt, P. R. Kubik, R. M. Marsolais, A. J. Berlinsky, and A. Landesman, *Phys. Rev. Lett.* **45**, 453 (1980).
- ¹¹Matheson Gas Products, P.O. Box 1587, Secaucus, NJ 07094.
- ¹²W. E. Bell, A. L. Bloom, and J. Lynch, *Rev. Sci. Instrum.* **32**, 688 (1961).
- ¹³A. Gallagher and E. H. Lewis, *J. Opt. Soc. Am.* **63**, 864 (1973).
- ¹⁴B. Khouw, J. E. Morgan, and H. I. Schiff, *J. Chem. Phys.* **50**, 66 (1969).
- ¹⁵K. M. Sancier and H. Wise, *J. Chem. Phys.* **51**, 1434 (1969).
- ¹⁶A. J. C. Varandas and M. C. A. Gomes, *Mol. Phys.* **45**, 317 (1982).
- ¹⁷E. A. Mason and T. R. Marrero, *Adv. At. Mol. Phys.* **6**, 155 (1970).
- ¹⁸L. C. Balling, R. J. Hanson, and F. M. Pipkin, *Phys. Rev.* **133**, A607 (1964); **135**, AB1 (1964).
- ¹⁹E. A. Mason, J. Ross, and P. N. Schatz, *J. Chem. Phys.* **25**, 626 (1956).
- ²⁰G. Das and S. Ray, *Phys. Rev. Lett.* **24**, 1391 (1970).
- ²¹W. H. Miller and H. F. Schaefer, *J. Chem. Phys.* **53**, 1421 (1970).
- ²²W. D. Davison and Y. C. Liew, *J. Phys. B* **5**, 309 (1972).
- ²³G. Das, A. F. Wagner, and A. C. Wahl, *J. Chem. Phys.* **68**, 4917 (1978).
- ²⁴R. Jochemsen, A. J. Berlinsky, and W. N. Hardy, *Can. J. Phys.* **62**, 751 (1984).
- ²⁵H. O'Hara and F. J. Smith, *J. Comput. Phys.* **5**, 328 (1970).
- ²⁶R. Gengenbach, Ch. Hahn, and J. P. Toennies, *Phys. Rev. A* **7**, 98 (1973).
- ²⁷R. A. Aziz and G. Scoles (private communication).